Supplemental material

Regulation of DNA-end resection by hnRNPU-like proteins promotes DNA double-strand break signaling and repair

Sophie E. Polo, Andrew N. Blackford, J. Ross Chapman, Linda Baskcomb, Serge Gravel, Andre Rusch, Anoushka Thomas, Rachel Blundred, Philippa Smith, Julia Kzhyshkowska, Thomas Dobner, A. Malcolm R. Taylor, Andrew S. Turnell, Grant S. Stewart, Roger J. Grand* and Stephen P. Jackson*

Supplementary figures

Supplementary tables (related to Experimental procedures)

Supplementary procedures

Supplementary references

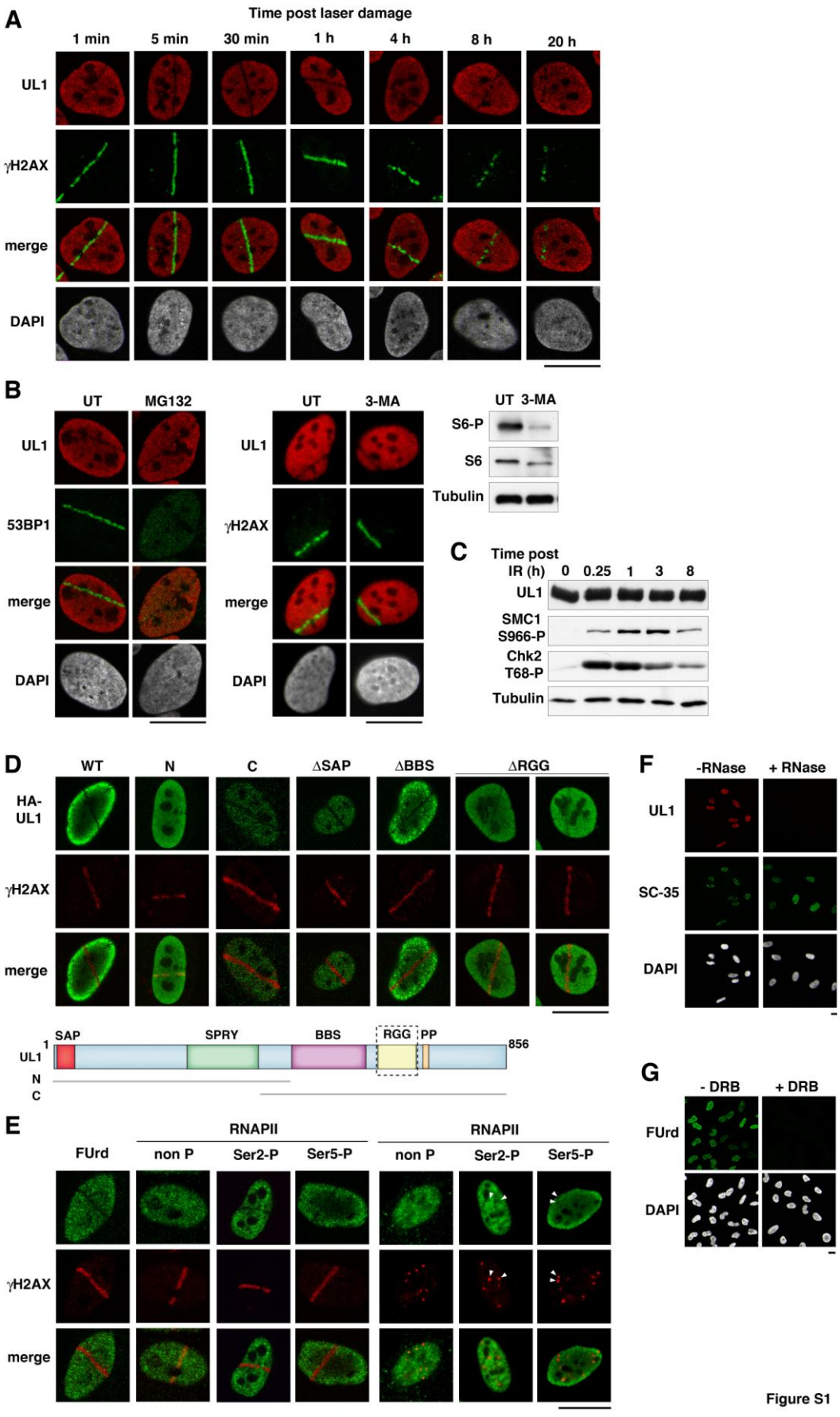
A
Time post laser damage
1 min
5 min
30 min
1 h
4 h
8 h
20 h
UL1
γH2AX
merge
DAPI
B
UT
MG132
UT
3-MA
UT
3-MA
UL1
53BP1
merge
DAPI
UL1
γH2AX
merge
DAPI
S6-P
S6
Tubulin
C
Time post IR (h)
0
0.25
1
3
8
UL1
SMC1 S966-P
Chk2 T68-P
Tubulin
D
WT
N
C
ΔSAP
ΔBBS
ΔRGG
HA-UL1
γH2AX
merge
SAP
SPRY
BBS
RGG
PP
1
856
UL1
N
C
E
FUrd
RNAPII
non P
Ser2-P
Ser5-P
RNAPII
non P
Ser2-P
Ser5-P
γH2AX
merge
F
-RNase
+ RNase
UL1
SC-35
DAPI
G
- DRB
+ DRB
FUrd
DAPI

Figure S1

Figure S1: hnRNPUL1 exclusion from sites of DNA damage is not due to protein degradation and is linked to inhibition of RNA synthesis (related to Figure 2)

(A) Immunodetection of hnRNPUL1 (UL1) and γH2AX at the indicated times after laser micro-irradiation in U2OS cells.

(B) Immunodetection of the indicated proteins 30 min after laser micro-irradiation in U2OS cells. MG132 treatment inhibits 53BP1 recruitment to DNA damage sites but does not prevent hnRNPUL1 exclusion. Likewise, cell treatment with the autophagy inhibitor 3-methyladenine (3-MA) inhibits phosphorylation of the ribosomal protein S6 (S6-P, control western-blot on the right; Codogno and Meijer, 2005) but does not impair hnRNPUL1 exclusion from laser tracks. UT: untreated.

(C) Western-Blot analysis of hnRNPUL1 protein levels in total extracts from HeLa cells at the indicated times after 10 Gy IR. SMC1 and Chk2 phosphorylations are used as DDR controls and Tubulin as loading control.

(D) Exclusion of HA-hnRNPUL1 wild-type (WT) or the indicated truncation mutants from sites of laser-induced damage (γHAX) 30 min after micro-irradiation in U2OS cells. hnRNPUL1 exclusion requires its carboxy-terminal domain and in particular the RGG-rich RNA-binding domain (dotted box). The scheme depicts the domain organization of hnRNPUL1 as in Figure 1.

(E) Local inhibition of RNA synthesis (visualized by FUrd incorporation) with exclusion of RNAPII phosphorylated forms (Ser2-P, Ser5-P) at sites of laser damage (30 min after micro-irradiation) and at IRIF (9 h post 10 Gy) in U2OS cells. Arrowheads indicate major IRIF.

(F) hnRNPUL1 subcellular localization is RNA-dependent. Immunodetection of hnRNPUL1 and the splicing factor SC-35 (RNase-resistant) in U2OS cells. hnRNPUL1 is solubilized upon RNase treatment and thus is washed away with the detergent that is used before fixation and immunostaining in this experiment.

(G) Effect of DRB treatment (100 μM for 2h) on RNA synthesis (FUrd) in U2OS cells. Scale bars, 10 μm.

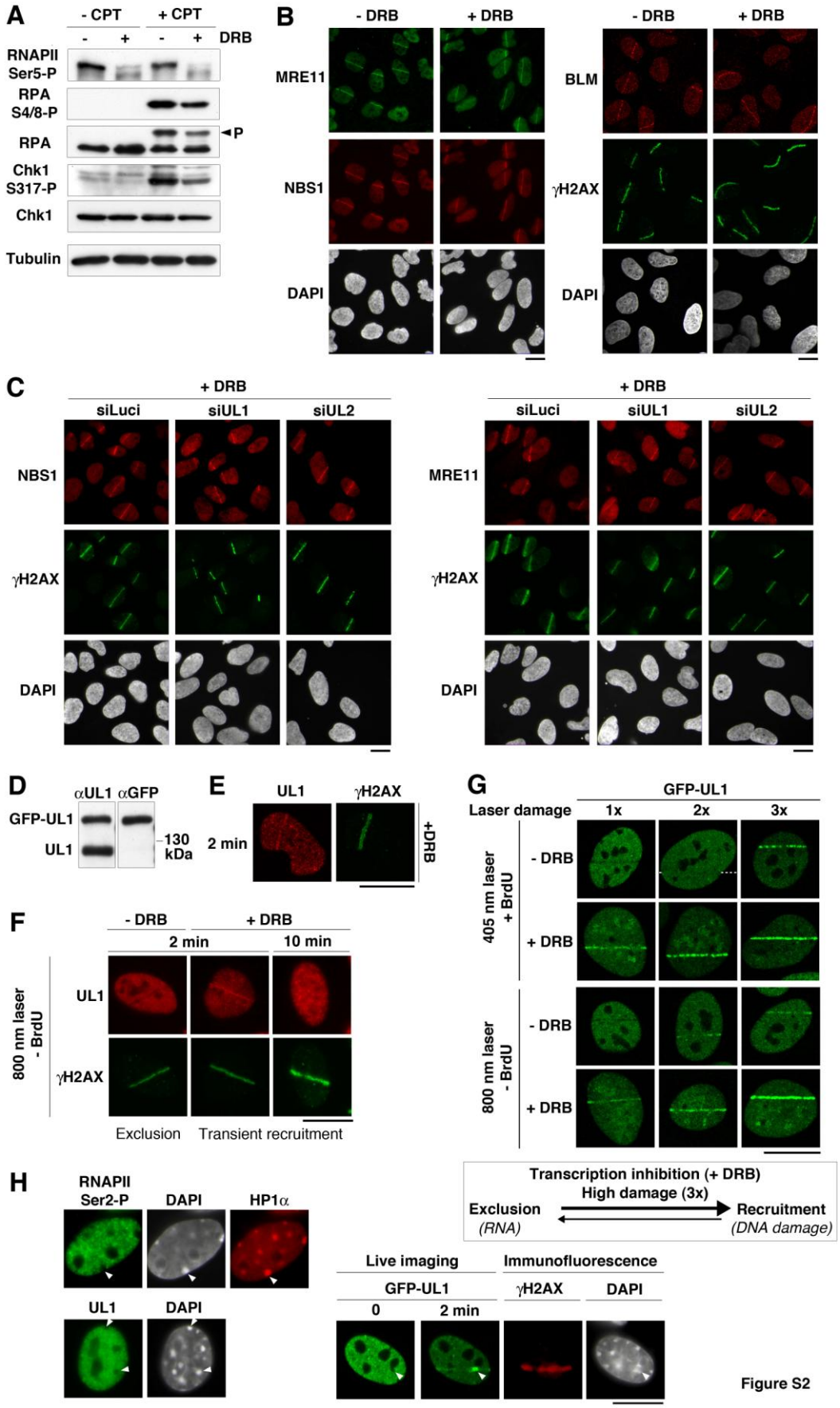
A
- CPT
+ CPT
DRB
RNAPII Ser5-P
RPA S4/8-P
RPA
P
Chk1 S317-P
Chk1
Tubulin
B
- DRB
+ DRB
MRE11
NBS1
DAPI
BLM
γH2AX
DAPI
C
+ DRB
siLuci
siUL1
siUL2
NBS1
γH2AX
DAPI
MRE11
γH2AX
DAPI
D
αUL1
αGFP
GFP-UL1
UL1
130 kDa
E
UL1
γH2AX
2 min
+DRB
F
- DRB
+ DRB
2 min
10 min
800 nm laser - BrdU
UL1
γH2AX
Exclusion
Transient recruitment
G
GFP-UL1
Laser damage
1x
2x
3x
405 nm laser + BrdU
- DRB
+ DRB
800 nm laser - BrdU
- DRB
+ DRB
H
RNAPII Ser2-P
DAPI
HP1α
UL1
DAPI
Transcription inhibition (+ DRB)
High damage (3x)
Exclusion
(RNA)
Recruitment
(DNA damage)
Live imaging
Immunofluorescence
GFP-UL1
γH2AX
DAPI
0
2 min

Figure S2

Figure S2: Effect of DRB on the cellular response to DSBs and hnRNPUL1 recruitment to DNA damage sites (related to Figure 2)

(A) Effect of DRB pre-treatment on the phosphorylation of DSB-response proteins analyzed by western-blotting on total extracts from U2OS cells 90 min after addition of 1 μM camptothecin (+CPT). P indicates RPA phosphorylated form. Phosphorylated RNAPII (RNAPII Ser5-P) is used as positive control for DRB treatment and Tubulin is used as loading control.

(B) Recruitment of BLM and MRN subunits to sites of laser-induced damage analyzed by immunofluorescence 1 h after micro-irradiation in U2OS cells pre-treated or not with DRB.

(C) Recruitment of MRN subunits to sites of laser-induced damage analyzed by immunofluorescence 1 h after micro-irradiation in U2OS cells treated with DRB and the indicated siRNAs.

(D) Western-blot analysis showing that U2OS cells stably express full-length GFP- hnRNPUL1 at levels similar to endogenous hnRNPUL1.

(E) Recruitment of endogenous hnRNPUL1 to sites of laser damage 2 min after micro-irradiation in U2OS cells.

(F) Transient recruitment of endogenous hnRNPUL1 to sites of DNA damage induced by 800 nm laser in the absence of BrdU pre-sensitization analyzed by immunofluorescence at the indicated times after micro-irradiation in U2OS cells pre-treated or not with DRB.

(G) Recruitment of GFP-hnRNPUL1 to sites of laser damage in U2OS cells 2 min after micro-irradiation under the indicated conditions. The dotted line in the top middle panel indicates the laser path. Recruitment of hnRNPUL1 takes over exclusion upon increased laser damage or when transcription is inhibited. Such distribution reflects the dual function of hnRNPUL proteins: these being preferentially engaged in the DDR or involved in RNA metabolism depending on the relative amounts of DNA damage and RNA synthesis.

(H) *Left:* Immunodetection of active RNAPII (phosphorylated on Ser2) and hnRNPUL1 (UL1) in mouse NIH3T3 cells. Arrowheads indicate major heterochromatin domains (DAPI dense and enriched in the heterochromatin protein HP1α), which are largely devoid of active RNAPII and hnRNPUL1. *Right:* Recruitment of GFP-hnRNPUL1 to sites of laser-induced damage analyzed at the indicated times after micro-irradiation in NIH3T3 cells without DRB pre-treatment. GFP-hnRNPUL1 preferentially accumulates at heterochromatin domains (DAPI-dense) along the laser tracks (marked by γH2AX). Note that heterochromatin structure is partially disrupted upon laser damage. Scale bars, 10 μm.

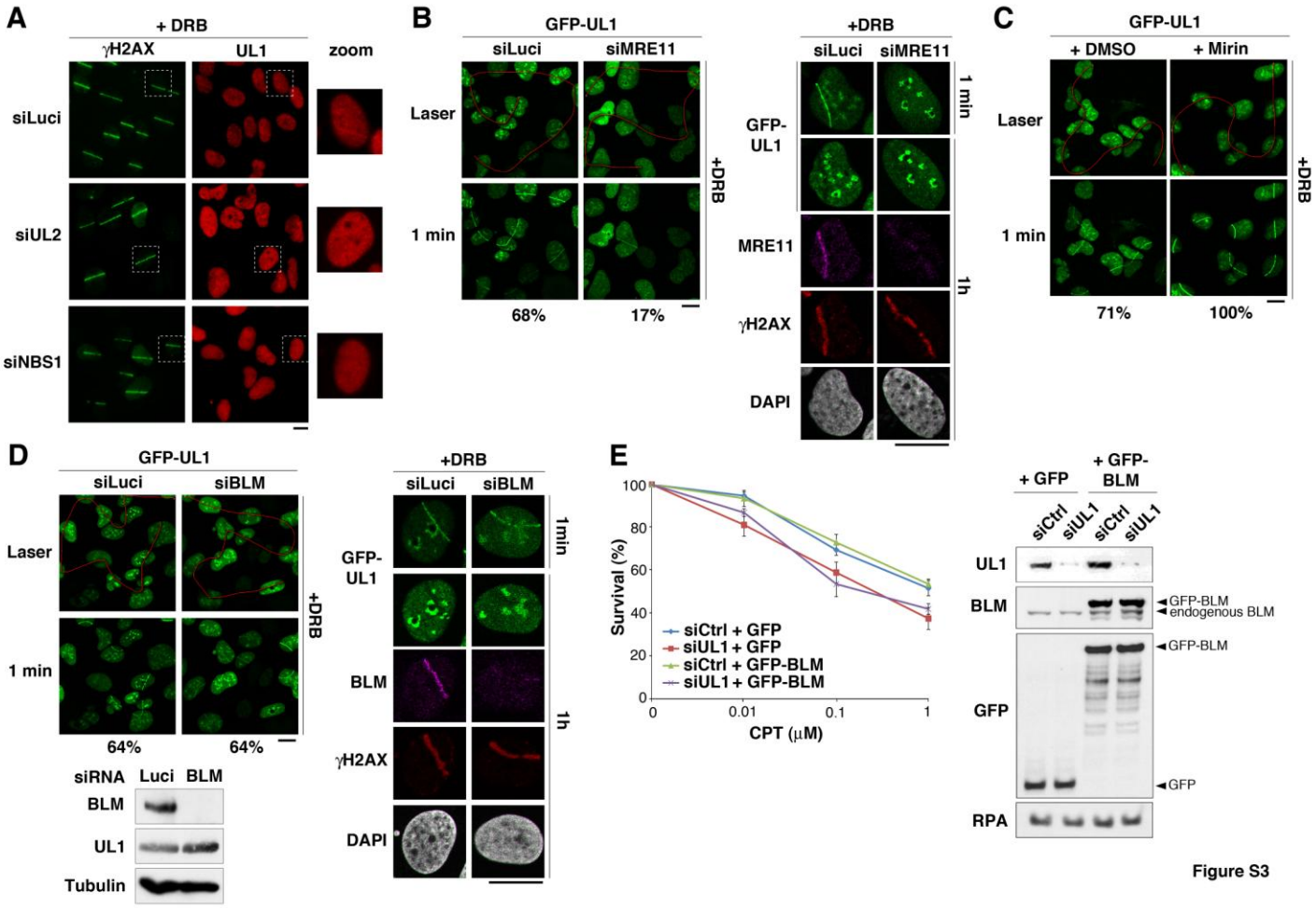

Figure S3: Role of the MRN complex and BLM in hnRNPUL1 function in response to DNA damage (related to Figures 2 and 5)

(A) Recruitment of endogenous hnRNPUL1 to sites of laser damage 2 min after micro-irradiation in U2OS cells treated with the indicated siRNAs (siLuci: control).

(B) GFP-hnRNPUL1 recruitment to sites of laser-induced damage (red line: laser path) analyzed by live cell imaging 1 min after micro-irradiation in U2OS cells treated with the indicated siRNAs. The efficiency of MRE11 depletion is confirmed by immunofluorescence on cells fixed 1 h after laser damage (right panel, where the top row represents the same cells by live imaging 1 min after laser micro-irradiation).

(C) GFP-hnRNPUL1 recruitment to sites of laser-induced damage is not impaired by cell treatment with MRN inhibitor (Mirin; DMSO: control).

(D) GFP-hnRNPUL1 recruitment to sites of laser-induced damage is not impaired by BLM depletion. The efficiency of BLM depletion is confirmed by western-blot (bottom) and by immunofluorescence (right panel, as in B). Percentages indicate the fraction of damaged cells showing GFP-hnRNPUL1 recruitment to laser lines (obtained by scoring at least 100 cells in two independent experiments). In all experiments, cells were pre-treated with DRB. Scale bars, 10 μm.

(E) Clonogenic survival of HeLa cells transfected with the indicated siRNAs (siCtrl: control) and plasmids (GFP: control or GFP-BLM: described in Hu et al., 2001) in response to camptothecin (CPT). Error bars indicate s.e.m. from 3 independent experiments. The expression levels of hnRNPUL1 and BLM for each condition are shown on the western-blot panel (right).

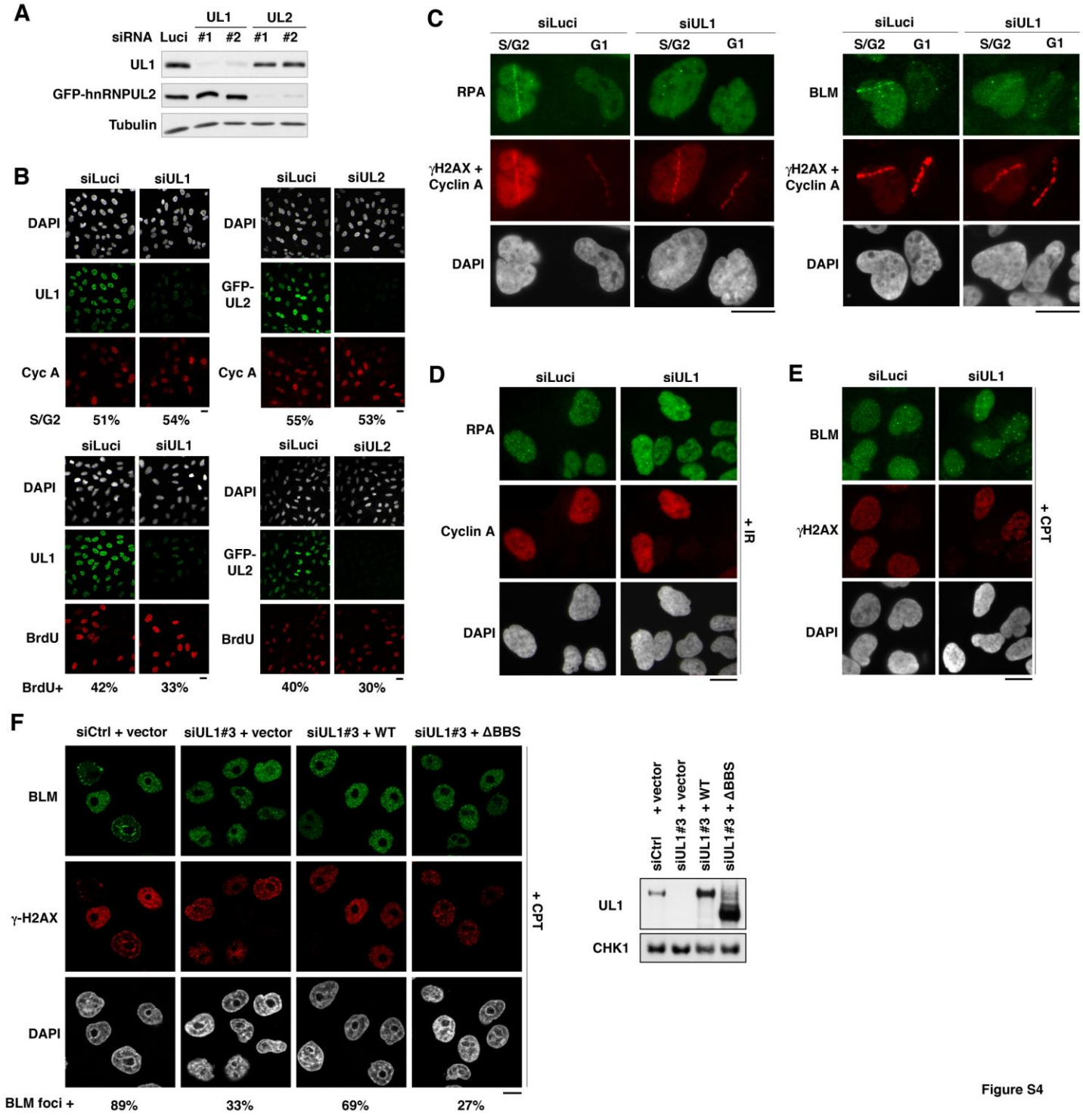

Figure S4

Figure S4: Effect of hnRNPUL protein depletion on the S/G2 cell population and on RPA and BLM recruitment to DNA damage sites in S/G2 (related to Figures 3, 4 and 5)

(A) Western-Blot analysis on total extracts from U2OS cells treated with the indicated siRNAs (Luci: control).

(B) Immunodetection of Cyclin A (S/G2 cells) and BrdU (replicating cells) upon hnRNPUL1 or hnRNPUL2 depletion compared to control (siLuci) in U2OS cells. Percentages indicate the

fraction of positive cells from scoring around 300 cells in each case. Similar results were obtained in 2 independent experiments.
(C) Recruitment of RPA and BLM to sites of laser-induced damage (γH2AX) in S/G2 cells (Cyclin A-positive) analyzed by immunofluorescence 1 h after micro-irradiation in U2OS cells treated with the indicated siRNAs.
(D) IR-induced RPA foci forming in S/G2 cells (Cyclin A-positive) analyzed in U2OS cells treated with the indicated siRNAs.
(E) CPT-induced BLM micro-foci forming in S phase cells (γH2AX-positive) analyzed in U2OS cells treated with the indicated siRNAs.
(F) CPT-induced BLM micro-foci forming in S phase cells (γH2AX-positive) analyzed in HeLa cells transfected with the indicated siRNAs and plasmids, as in Figure 4C. Percentages indicate the proportions of γH2AX-positive cells showing BLM micro-foci from scoring around 150 cells in each case. The expression levels of hnRNPUL1 in each condition are shown on the western-blot panel (right). Scale bars, 10 μm.

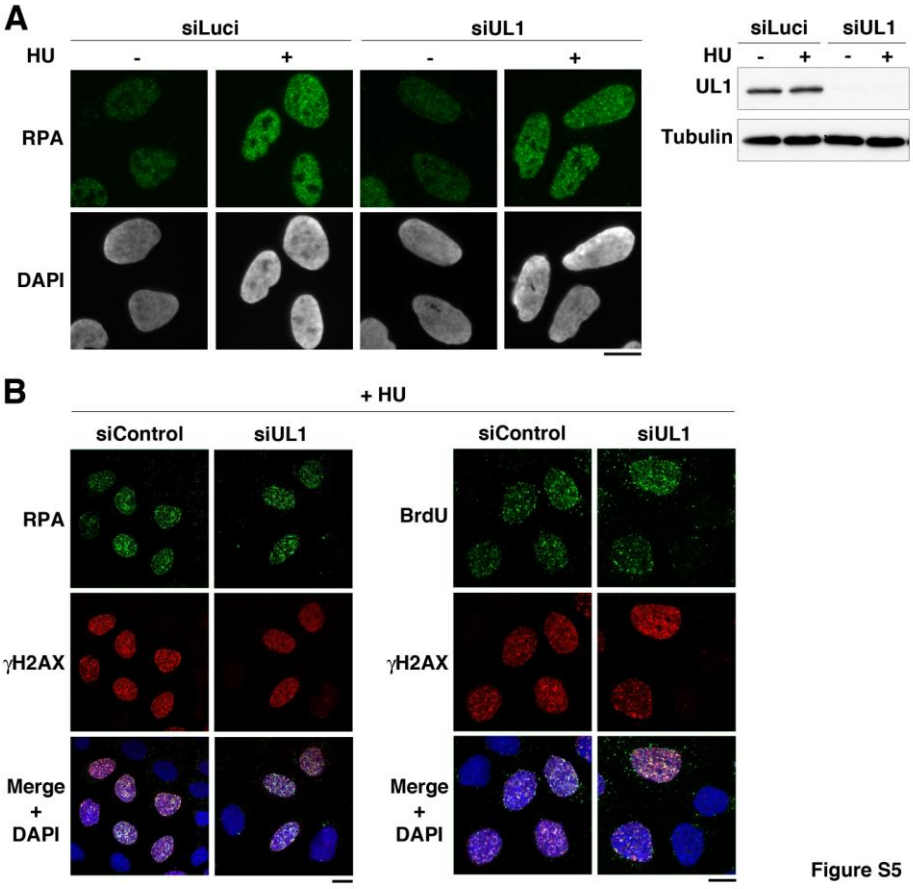

Figure S5: hnRNPUL proteins are not involved in response to replication stress (related to Figure 4)
hnRNPUL1 depletion does not impair RPA accumulation or ssDNA formation (BrdU) upon replication stress (HU treatment) in U2OS **(A)** or HeLa cells **(B)**. Similar results were obtained upon hnRNPUL2 depletion (not shown). Scale bars, 10 μm.

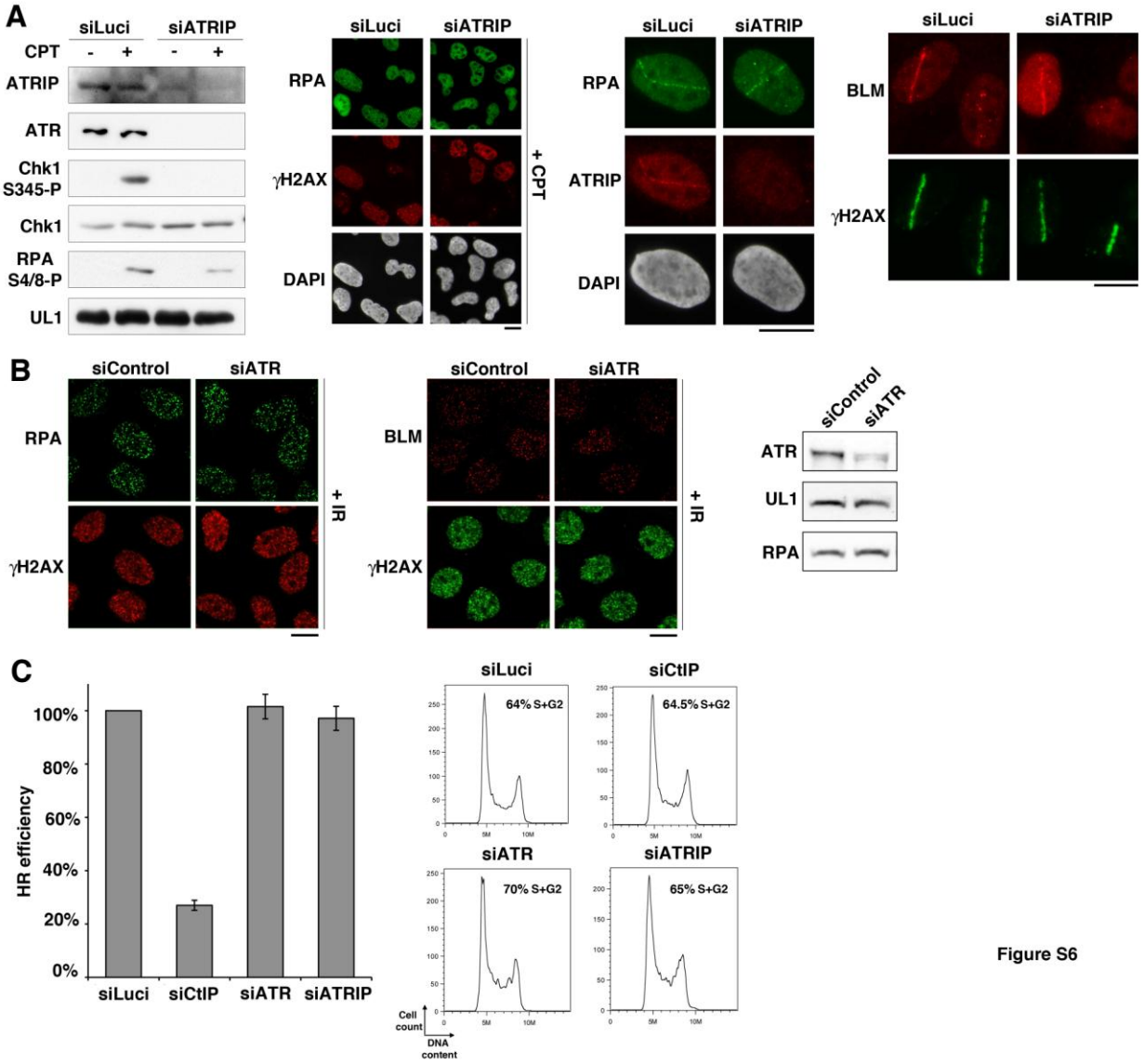

Figure S6

Figure S6: Inhibition of ATR signaling does not impinge on resection and HR (related to Figures 3 and 5)

(A) ATRIP depletion in U2OS cells inhibits ATR-dependent signaling (ATR is destabilized, Chk1 is not phosphorylated upon DNA damage) but it does not abrogate RPA phosphorylation or focus-formation upon camptothecin treatment (CPT), and it does not affect RPA or BLM recruitment to laser-induced damage.

(B) ATR depletion in HeLa cells does not affect RPA or BLM accumulation at sites of IR-induced damage. Scale bars, 10 μm.

(C) HR-mediated gene conversion assay. HR efficiencies are normalized to siLuci. Error bars: s.d. from 3 independent experiments. CtIP depletion is used as a positive control. Corresponding FACS profiles show no major effect of siRNA treatments on S/G2 cell populations; proportions of cells in S/G2 were estimated by the Dean/Jett/Fox model with FlowJo software.

Table S1: siRNA sequences

siRNA	Target sequence
ATR	described in (Blackford et al., 2008)
ATRIP	5' AGAGAAACUGUUCCAAUUA 3' (MWG-Biotech)
BLM	SMARTpool described in (Gravel et al., 2008)
Control	AllStars Negative Control siRNA (Qiagen) or ON-TARGETplus Non-Targeting Pool (Dharmacon)
CtIP	5' GCUAAAACAGGAACGAAUC 3' (MWG-Biotech) or SMARTpool (Dharmacon)
EXO1	SMARTpool (Dharmacon)
Luciferase	5' CGUACGCGGAAUACUUCGA 3' (MWG-Biotech)
MRE11	5' GAGCAUAACUCCAUAAGUA 3' (MWG-Biotech) or SMARTpool (Dharmacon)
NBS1	5' GGAAGAAACGUGAACUCAA 3' (MWG-Biotech)
UL1 #1	5' GCAGUGGAACCAGUACUAU 3' (MWG-Biotech)
UL1 #2	5' CACCUCCCUUGAUCAUACA 3' (MWG-Biotech)
UL1#3	5' GAGAGUGACUAUUGAACUU 3' and 5' CCUCCCUUGAUCAUACAGU 3' (Dharmacon); 1:1 combination targeting hnRNPUL1 3'UTR
UL2 #1	5' UGGCCGAGCUUACUAUGAA 3' (MWG-Biotech)
UL2 #2	5' GAGGAAGAUUGGAAGAAGA 3' (MWG-Biotech)

Table S2: Plasmids

Plasmid encoding	Origin
GST-NBS1 Nt and Ct	(Yuan et al., 2007)
GST-hnRNPUL1	(Gabler et al., 1998)
HA-hnRNPUL1 wt and deletion mutants (N, M, C, ΔBBS (#2), ΔRGG)	(Barral et al., 2005; Kzhyshkowska et al., 2003; Kzhyshkowska et al., 2001)
HA-hnRNPUL1-ΔSAP (aa 101-856)	NcoI/XhoI fragment of HA-hnRNPUL1 wt plasmid ligated with the HA-tag expression cassette and subcloned into pcDNA3 (Invitrogen)
GST-BBS-RGG region of hnRNPUL1 (aa 445-695)	BBS-RGG region of hnRNPUL1 subcloned into pGEX4T1 (GE Healthcare)
BBS-RGG for IVT	BBS-RGG region of hnRNPUL1 subcloned into pcDNA3 (Invitrogen)
GFP-HA-hnRNPUL1	GFP sequence PCR-amplified from pEGFP-C1 (Clontech) included upstream of the HA sequence in HA-hnRNPUL1 wt construct
GFP-hnRNPUL2	RT-PCR-amplified hnRNPUL2 cDNA from MRC5 cells cloned into pEGFP-C1 (Clontech)
GST-hnRNPUL2	hnRNPUL2 sequence subcloned into pGEX-4T-1 (GE Healthcare)
hnRNPUL2 for IVT	hnRNPUL2 sequence subcloned into pcDNA3 (Invitrogen)
NBS1 for IVT	full-length human NBS1 sequence cloned into pSG5 (Stratagene)
RAD50 for IVT	(Gatei et al., 2011)
MRE11 for IVT	J. Petrini
GFP-EXO1	human EXO1 cDNA (Geneservice) subloned into pEGFP-C1 (Clontech)

wt: wild-type ; aa: amino acids ; IVT: *in vitro* translation

Table S3: Primary antibodies

Antibody target	Species	Supplier/Reference	Application
53BP1	rabbit	NB100-304 (Novus Biologicals)	IF
ATR	goat	sc-1887 (Santa-cruz)	IB
ATR	mouse	ab4471 (Abcam)	IB
ATRIP	rabbit	A300-095A (Bethyl)	IF, IB
β-actin	mouse	A2228 (Sigma)	IB
BLM	rabbit	(Moens et al., 2000)	IB
BLM	rabbit	A300-110A (Bethyl)	IF
BLM	goat	sc-7790 (Santa-cruz)	IF, IP
BRCA1	mouse	sc-6954 (Santa-cruz)	IF
BrdU	mouse	RPN202 (Amersham)	IF
Chk1	mouse	sc-8408 (Santa-cruz)	IB
Chk1-S345-P	rabbit	2348 (Cell Signaling)	IB
Chk2	rabbit	ab8108 (Abcam)	IB
Chk2 T68-P	rabbit	DR-1026 (Calbiochem)	IB
CtIP	mouse	#14-1 from R. Baer (Yu and Baer, 2000)	IF, IB, IP
Cyclin A	rabbit	sc-751 (Santa-cruz)	IF
Cyclin A	mouse	611268 (BD Biosciences)	IF, IB
FUrd	mouse	B-8434 (Sigma)	IF
γH2AX	mouse	05-636 (Upstate)	IF, IB
γH2AX	rabbit	2577 (Cell Signaling)	IF, IB
GFP	mouse	7.1/13.1 (Roche)	IB, IP
H2AX	rabbit	ab11175 (Abcam)	IB
HA	mouse	MMS101R (Covance)	IF
hnRNPUL1	rabbit	Ab-1 (#960; Blackford et al., 2008) Ab-2 (#961; this study)	IF, IB, IP
hnRNPUL1	rat	6C5 (Kzhyshkowska et al., 2001)	IB
HP1α	mouse	2HP-1H5-As (Euromedex)	IF
MDC1	mouse	M2444 (Sigma)	IF
MRE11	mouse	ab214 (Abcam)	IF, IP
MRE11	rabbit	NB100 (Novus)	IB
NBS1	mouse	ab7860 (Abcam)	IB, IP
NBS1	rabbit	NB100-143 (Novus Biologicals)	IF
Nucleolin	rabbit	sc-13057 (Santa-cruz)	IF
RAD50	mouse	ab4184 (Abcam)	IB, IP
RNAPII non-P	mouse	ab817 (Abcam)	IF
RNAPII Ser2-P	rabbit	ab5095 (Abcam)	IF
RNAPII Ser5-P	mouse	ab5408 (Abcam)	IF
RPA	mouse	ab2175 (Abcam)	IF, IB
RPA S4/8-P	rabbit	A300-245A (Bethyl)	IF, IB
S6	rabbit	2217 (Cell Signaling)	IB
S6-P	rabbit	2215 (Cell Signaling)	IB
Sc-35	mouse	S4045 (Sigma)	IF
SMC1 S966-P	rabbit	A300-050A (Bethyl)	IB
Tubulin	mouse	T9026 (Sigma)	IB

IF: Immunofluorescence, IB: Immunoblot, IP: Immunoprecipitation

Table S4: Drug treatments

Drug	Purpose	Supplier	Conditions of use [a]
CPT (Camptothecin)	Topoisomerase I poison; DSBs in S phase	Sigma-Aldrich	1 μM for indicated time
HU (Hydroxyurea)	Replication stress	Sigma-Aldrich	2 mM or 3 mM for 1h
Mirin (Dupre et al., 2008)	MRE11 inhibitor	J. Gautier	50 μM for 1h
DRB (5,6 dichloro-β-D-ribofuranosylbenzimidazole)	Transcription inhibitor	Sigma-Aldrich	100 μM for 2-4h
MG132	Proteasome inhibitor	Merck	25 μM for 1h30
3-methyladenine (Seglen and Gordon, 1982)	Autophagy inhibitor	Invivogen	10 mM final for 1h30
BrdU (5-bromo-2'-deoxyuridine)	ssDNA detection	Sigma-Aldrich	10 μM for 24h
FUrd (5-Fluoro-uridine)	Detection of newly synthesized RNA	Sigma-Aldrich	1 mM for 15 min

[a]Final concentrations in culture medium are indicated

Supplementary procedures

Cell culture conditions

Human U2OS, HEK-293, HeLa and A549 cells, and mouse NIH3T3 cells were grown in Dulbecco's modified Eagle medium (Invitrogen) supplemented with 10% fetal bovine serum (FBS; BioSera), 2mM L-glutamine, 100 unit/ml penicillin, 100 μg/ml streptomycin and fungizone (Sigma-Aldrich). U2OS DR-GFP cells were cultured in the same medium supplemented with 1 μg/ml puromycin (Sigma-Aldrich). LCLs were grown in RPMI medium supplemented with 10% FBS, penicillin and streptomycin. Stable cell lines were established by selection in medium containing 0.5 mg/ml G418 (Invitrogen).

Laser micro-irradiation

Cells plated on glass-bottom dishes (Willco Wells) were pre-sensitized with 10 μM 5-bromo-2'-deoxyuridine (BrdU, Sigma-Aldrich) in phenol red-free medium (Invitrogen) for 24 h at 37°C. Micro-irradiation was performed with a FluoView 1000 confocal microscope (Olympus) equipped with a 37°C heating stage (Ibidi) and a 405 nm laser diode (6 mW) focused through a 60X UPlanSApo/1.35 oil objective to yield a spot size of 0.5-1 μm. Time of cell exposure to the laser beam was ~250 ms (fast scanning mode). Laser settings (SIM scanner, 0.40 mW output, 50 scans or 150 scans for hnRNPUL recruitment analyses) were chosen to generate a detectable DDR restricted to the laser path in a pre-sensitization-dependent manner without major cytotoxic effects. When indicated, cell pre-sensitization with BrdU was omitted and damage was introduced with a multiphoton laser (MaiTai, 800 nm, maximum power 2.8 W) through a Plan-Apochromat 63X/1.4 oil objective using a LSM710 NLO confocal microscope (Zeiss) and the following laser settings: 6% power, 1 iteration, scan speed 12.6 μsec/pixel.

Immunofluorescence

Cells on glass coverslips (VWR) or glass-bottom dishes (Willco Wells) were fixed with 2% paraformaldehyde and permeabilized with 0.2 % Triton-X-100 in PBS. Samples were blocked in 5% bovine serum albumin and stained with the appropriate primary (Table S3) and secondary antibodies coupled to AlexaFluor 488/594/647 (Molecular Probes) or to FITC/Rhodamine/Cyanine5 (Jackson Immunoresearch). For BrdU immunodetection in dsDNA (replicating cells), a 10 min-denaturation step with HCl 4N was included prior to blocking. Cell

preparations were mounted in Vectashield with DAPI (Vector labs). Confocal images were captured on a Nikon Eclipse E800 microscope equipped with Radiance 2100 laser set-up and LaserSharp software (BioRad) or on FluoView1000 Olympus using a 40X or 60X oil objective. To avoid bleed-through effects in double-staining experiments, each dye was scanned independently in a multi-tracking mode.

Immunoblotting

Total cell extracts were obtained by scraping cells in Laemmli buffer (0.8% SDS, 4% glycerol, 280 mM β-mercaptoethanol, 25 mM Tris-HCl pH 6.8, 0.005% bromophenol blue). Proteins were resolved by SDS-PAGE, transferred onto nitrocellulose (Protran) and probed using the appropriate primary (Table S3) and secondary antibodies coupled to horse-radish peroxidase (Dako, Pierce). Protein detection was done with ECL reagents (GE Healthcare).

Immunoprecipitation

Cells harvested in PBS were lysed in 20 mM Tris pH 7.5, 40 mM NaCl, 2 mM $MgCl_2$, 0.5% NP-40, 50 U/ml benzonase, supplemented with protease and phosphatase inhibitors and adjusted to 150 or 450 mM salt concentration. Lysates were clarified by centrifugation (13200 rpm, 20 min, 4°C) and at least 1 mg proteins were used per immunoprecipitation in IP buffer (25 mM Tris pH 7.5, 150 mM NaCl, 1.5 mM DTT, 10% glycerol, 0.5% NP-40) supplemented with protease and phosphatase inhibitors. Endogenous proteins were captured onto protein G-Dynabeads (Dynal) coupled to the indicated antibody, while GFP-tagged proteins were captured onto GFP-Trap agarose beads (ChromoTek) or protein G-Dynabeads coupled to anti-GFP antibody (Table S3). Complexes were extensively washed in IP buffer. Immunoprecipitation with non specific IgG or from cells expressing GFP only was used as negative control.

Colony forming assays

Three days after siRNA transfection, cells were replated and exposed to the indicated DNA damaging agent the following day. After an additional 14-day incubation, colonies were stained with 0.5% crystal violet/20% ethanol and counted. Results were normalized to plating efficiencies to focus on the effect of hnRNPUL depletion after DNA damage (note that in the absence of DNA-damaging agent, the viability of hnRNPUL-depleted cells is at least 50% of that of control cells).

Homologous recombination assays

A U2OS cell line with the integrated HR reporter DR-GFP (gift from M. Jasin, generated as described in (Pierce et al., 2001) was transfected with the indicated siRNAs. Three days later, cells were co-transfected with the I-*Sce*I expression vector pCBA-I-*Sce*I (Pierce et al., 1999) and a vector expressing monomeric red fluorescent protein (pRFP-C1, R.Y. Tsien). The latter plasmid was added at a 1:5 ratio to mark transfected cells. Cells were harvested two days later and subjected to FACS analysis to determine the efficiency of homologous recombination-mediated gene conversion (HR efficiency) induced by I-*SceI* digestion, which reconstitutes a functional GFP gene. DAPI was added to the cells to label and gate out dead cells. FACS data were obtained on a MoFlo analyser equipped with Summit V4.3 software to reveal the percentage of dual RFP- and GFP-positive cells (i.e. transfected and HR proficient). Results were corrected for transfection efficiency and normalized to siLuciferase control cells after subtraction of background HR efficiency, obtained from U2OS DR-GFP cells transfected with pRFP-C1 only.

Supplementary references

Barral, P.M., Rusch, A., Turnell, A.S., Gallimore, P.H., Byrd, P.J., Dobner, T., and Grand, R.J. (2005). The interaction of the hnRNP family member E1B-AP5 with p53. FEBS Lett *579*, 2752-2758.

Blackford, A.N., Bruton, R.K., Dirlik, O., Stewart, G.S., Taylor, A.M., Dobner, T., Grand, R.J., and Turnell, A.S. (2008). A role for E1B-AP5 in ATR signaling pathways during adenovirus infection. J Virol *82*, 7640-7652.

Codogno, P., and Meijer, A.J. (2005). Autophagy and signaling: their role in cell survival and cell death. Cell Death Differ *12 Suppl 2*, 1509-1518.

Dupre, A., Boyer-Chatenet, L., Sattler, R.M., Modi, A.P., Lee, J.H., Nicolette, M.L., Kopelovich, L., Jasin, M., Baer, R., Paull, T.T., and Gautier, J. (2008). A forward chemical genetic screen reveals an inhibitor of the Mre11-Rad50-Nbs1 complex. Nat Chem Biol *4*, 119-125.

Gabler, S., Schutt, H., Groitl, P., Wolf, H., Shenk, T., and Dobner, T. (1998). E1B 55-kilodalton-associated protein: a cellular protein with RNA-binding activity implicated in nucleocytoplasmic transport of adenovirus and cellular mRNAs. J Virol *72*, 7960-7971.

Gatei, M., Jakob, B., Chen, P., Kijas, A.W., Becherel, O.J., Gueven, N., Birrell, G., Lee, J.H., Paull, T.T., Lerenthal, Y*., et al.* (2011). ATM-dependent phosphorylation of RAD50 regulates DNA repair and cell cycle control. J Biol Chem *286*, 31542-31556.

Gravel, S., Chapman, J.R., Magill, C., and Jackson, S.P. (2008). DNA helicases Sgs1 and BLM promote DNA double-strand break resection. Genes Dev *22*, 2767-2772.

Hu, P., Beresten, S.F., van Brabant, A.J., Ye, T.Z., Pandolfi, P.P., Johnson, F.B., Guarente, L., and Ellis, N.A. (2001). Evidence for BLM and Topoisomerase IIIalpha interaction in genomic stability. Hum Mol Genet *10*, 1287-1298.

Kzhyshkowska, J., Rusch, A., Wolf, H., and Dobner, T. (2003). Regulation of transcription by the heterogeneous nuclear ribonucleoprotein E1B-AP5 is mediated by complex formation with the novel bromodomain-containing protein BRD7. Biochem J *371*, 385-393.

Kzhyshkowska, J., Schutt, H., Liss, M., Kremmer, E., Stauber, R., Wolf, H., and Dobner, T. (2001). Heterogeneous nuclear ribonucleoprotein E1B-AP5 is methylated in its Arg-Gly-Gly (RGG) box and interacts with human arginine methyltransferase HRMT1L1. Biochem J *358*, 305-314.

Moens, P.B., Freire, R., Tarsounas, M., Spyropoulos, B., and Jackson, S.P. (2000). Expression and nuclear localization of BLM, a chromosome stability protein mutated in Bloom's syndrome, suggest a role in recombination during meiotic prophase. J Cell Sci *113*, 663-672.

Pierce, A.J., Hu, P., Han, M., Ellis, N., and Jasin, M. (2001). Ku DNA end-binding protein modulates homologous repair of double-strand breaks in mammalian cells. Genes Dev *15*, 3237-3242.

Pierce, A.J., Johnson, R.D., Thompson, L.H., and Jasin, M. (1999). XRCC3 promotes homology-directed repair of DNA damage in mammalian cells. Genes Dev *13*, 2633-2638.

Seglen, P.O., and Gordon, P.B. (1982). 3-Methyladenine: specific inhibitor of autophagic/lysosomal protein degradation in isolated rat hepatocytes. Proc Natl Acad Sci U S A *79*, 1889-1892.

Yu, X., and Baer, R. (2000). Nuclear localization and cell cycle-specific expression of CtIP, a protein that associates with the BRCA1 tumor suppressor. J Biol Chem *275*, 18541-18549.

Yuan, Z., Zhang, X., Sengupta, N., Lane, W.S., and Seto, E. (2007). SIRT1 regulates the function of the Nijmegen breakage syndrome protein. Mol Cell *27*, 149-162.